

Article

# Surface Plasmon Resonance and Bending Loss-Based U-Shaped Plastic Optical Fiber Biosensors

Ariadny da S. Arcas <sup>1</sup>, Fábio da S. Dutra <sup>1,2</sup> , Regina C. S. B. Allil <sup>3</sup> and Marcelo M. Werneck <sup>1,3,\*</sup> 

<sup>1</sup> Nanotechnology Engineering Program, Universidade Federal do Rio de Janeiro, Rio de Janeiro 21941-901, Brazil; ariadny@lif.coppe.ufrj.br (A.d.S.A.); fabiodutra@petrobras.com.br (F.d.S.D.)

<sup>2</sup> Petrobras' Research and Development Center, CENPES, Rio de Janeiro 21941-915, Brazil

<sup>3</sup> Electrical Engineering Program, COPPE, Universidade Federal do Rio de Janeiro, Rio de Janeiro 21941-901, Brazil; regina@lif.coppe.ufrj.br

\* Correspondence: werneck@lif.coppe.ufrj.br; Tel.: +55-21-3938-8200

Received: 22 November 2017; Accepted: 8 February 2018; Published: 22 February 2018

**Abstract:** *Escherichia coli* (*E. coli*) is a large and diverse bacteria group that inhabits the intestinal tract of many mammals. Most *E. coli* strains are harmless, however some of them are pathogenic, meaning they can make one sick if ingested. By being in the feces of animals and humans, its presence in water and food is used as indicator of fecal contamination. The main method for this microorganism detection is the bacterial culture medium that is time-consuming and requires a laboratory with specialized personnel. Other sophisticated methods are still not fast enough because they require sending samples to a laboratory and with a high cost of analysis. In this paper, a gold-coated U-shaped plastic optical fiber (POF) biosensor for *E. coli* bacteria detection is presented. The biosensor works by intensity modulation principle excited by monochromatic light where the power absorption is imposed by predominant effect of either bending loss or surface plasmon resonance (SPR), depending on the gold thickness. Bacterial selectivity is obtained by antibody immobilization on the fiber surface. The biosensor showed a detection limit of  $1.5 \times 10^3$  colony-forming units (CFU)/mL, demonstrating that the technology can be a portable, fast response and low-cost alternative to conventional methodologies for quality analysis of water and food.

**Keywords:** biosensor; bacteria detection; bending loss; U-shaped fiber sensor; *Escherichia coli*; plastic optical fiber; refractive index; surface plasmon resonance

## 1. Introduction

Annually, thousands of people are hospitalized for foodborne illnesses, and some so severe that they result in death [1]. Foodborne diseases have increased significantly worldwide [2] having been motivated by several factors such as poor sanitation and food hygiene [3], population growth and disorderly urbanization, manufacturing contamination in industry due to bad practices, and the need for large-scale food production [4,5].

Among the microorganisms that cause foodborne diseases, the most common is the *Escherichia coli* (also known as *E. coli*) bacterium. *E. coli* is a large and diverse bacteria group that usually inhabits the intestinal tract of humans and other warm-blooded mammals. Most *E. coli* strains are harmless, however others are pathogenic, meaning that they can produce some kind of sickness if ingested [6]. By being in the feces of animals and humans, its presence in water and food is used as an indicator of fecal contamination.

The most common routes of *E. coli* contamination are drinking water, vegetables, undercooked meat, unpasteurized milk, and by bathing in polluted rivers and seas [7,8]. Its importance as a public health problem is evident in *E. coli* outbreaks such as those that occurred in July 1996 in Osaka schools,

Japan [9–11], in 1982 in the Oregon and Michigan cities, United States [12], and in May 2000 in the Ontario Walkerton farming community, Canada [13].

The main method for this microorganism detection is bacterial culture medium, which is time-consuming and requires a laboratory with specialized personnel. Other sophisticated methods are still not fast enough because they require sending samples to a laboratory, and involve high cost of analysis [14–17].

In this sense, great efforts are being made in the last two decades to develop new portable, fast-response, and reliable biosensor technologies for substituting conventional detection methods. Among these, optical technology has emerged on the market as a powerful, cheap and reliable tool allowing for the development of new techniques for biological detection.

Optical biosensors offer several advantages when compared with their conventional electric counterparts such as electric passiveness, long distance sensing, the possibility of multiplexing several sensing channels, electromagnetic immunity, etc. Baccar et al. [18], for instance, developed a simple low cost nanobiosensor by surface plasmon resonance (SPR) with a gold thin film deposited on a prism for *E. coli* detection with a detection limit of  $10^3$  colony-forming units CFU/mL. Geng et al. [16], as example, developed a fiber optic biosensor by evanescent wave absorption for *E. coli* O157:H7 detection in minced meat. The biosensor was able to measure  $10^4$  CFU/mL of bacteria concentration after four hours. Wandermur et al. [19] created a plastic optical fiber (POF) biosensor to detect *E. coli* O55 by evanescent wave (EW) principle. The sensor's detection limit was  $10^4$  CFU/mL after 60 min. Halkare et al. [20] produced a localized surface plasmon resonance (LSPR) based on a U-shaped fiber-optic probe for detection of *E. coli* B40 using bacteriophage T4. The sensor was able to detect a bacteria concentration of  $10^8$  CFU/mL.

This work presents a POF sensor coated with gold thin film for *E. coli* detection as a portable, fast response and low-cost alternative to conventional detection methodologies. The biosensor was manufactured in a U-shaped format and works by intensity-modulation principle excited by a monochromatic light that is attenuated by bending loss and SPR.

The U-shaped POF sensor detects the changes in the refractive index (RI) of the surrounding medium. The sensor is functionalized with *E. coli* antibodies attached to the gold thin film. When bacteria are present in the sample, they become attached to the sensor's surface, increasing the RI and changing the SPR resonance frequency.

The biosensor was experimentally tested under several bacteria concentrations and presented a detection limit of  $1.5 \times 10^3$  CFU/mL, demonstrating that the technology might be an efficient tool for quality analysis of water and food.

## 2. Working Principle

A bacterium presents a RI about 1.39 at 400–800 nm [15,21,22], slightly higher than that of pure water (1.333). Nonetheless, even in heavily contaminated water, with  $10^8$  CFU/mL, for instance, the bacteria concentration is not high enough to substantially change the RI of the water. Therefore, in order to detect bacteria by RI sensing, the detection system needs to concentrate the target bacteria around the fiber.

The technique known as immunocapture consists in covalently bonding the specific antibody on the sensor sensitive region in such a way that only bacteria of specific species are captured and fixed on the sensor surface [19,23,24].

The proposed sensor works by the measurement principle of optical power loss in a U-shaped POF. The light conducted by the optical fiber is attenuated, depending on the refractive index of the medium surrounding the sensor. In the shaped region, two effects cause light power losses: bending loss and SPR. SPR is the resonant oscillation of conduction electrons at the interface between a noble metal and a dielectric material, stimulated by incident light [25,26]. The SPR effect depends on the light wavelength, the incident angle, film thickness, and the surrounding RI [27–29].

In a multimode optical fiber, the light propagation takes place by the principle of total internal reflection (TIR); as a consequence, the incidence angle of the traveling optical ray is required to be higher than that of the critical angle. In the core-cladding interface, an EW is generated that extends with a range from 50–1000 nm into the cladding depending on the wavelength, the refractive index, and the angle of incidence [30].

At a fiber bend, the higher order propagation modes (the guided light rays reflecting at angles close to the critical angle) reach the core-cladding interface at an angle smaller than the critical one, and refract into the cladding instead of reflecting by TIR. At the cladding interface with the surrounding medium, there is another critical angle, so that all cladding modes that reach this interface at smaller angles are lost into the surrounding medium. Thus, an increase in RI in the surrounding of a U-shaped POF increases the critical angle of the cladding interface, which results in decreasing the V number (maximum number of modes allowed inside the fiber) and, as a consequence, more attenuation of the light. The attenuation phenomenon by the fiber bend is known as bending loss. An illustration of the bare U-shaped POF probe operating by bending loss effect in the presence of bacteria is showed in Figure 1 [23,31–34].

By covering the U-shaped POF probes with gold film, if the layer is thin enough to be transparent to some wavelengths, the attenuation is still predominantly imposed by the effect of bending loss. In this case, the sensor can be used in the same way as a pristine fiber, but it is endowed with a layer of gold for better immobilization of antibodies. However, for specific wavelengths, the SPR effect absorbs these wavelengths, causing light attenuation.

An illustration of a gold-coated U-shaped POF probe operating by the SPR effect in the presence of bacteria is shown in Figure 1.

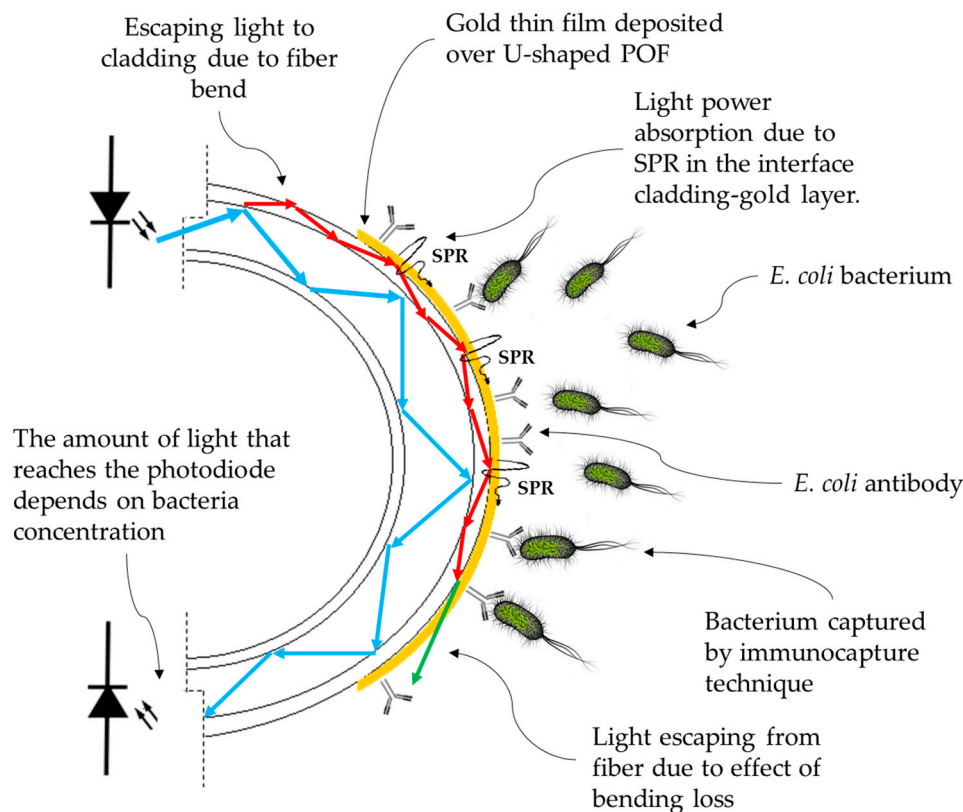


**Figure 1.** Illustration of the U-shaped gold-coated biosensor working principle.

### 3. Materials and Methods

#### 3.1. Probe Fabrication

U-shaped probes were fabricated using Mitsubishi Rayon Eska GH 4001 multi-mode POF 1 mm in diameter and a cladding thickness of 10  $\mu\text{m}$ . The core material was polymethyl methacrylate (PMMA) with RI = 1.49 in the visible range and the cladding material was fluorinated polymer with RI = 1.41. The fabrication process consisted of cutting the POF into approximately 10 cm-long sections, and both end surfaces were cleaved and polished for maximum light coupling. Then, the 10 cm-long sections were shaped and placed in a manually operated custom-made device (Figure 2a) for molding the U-shaped POF in a curve with 8 mm in diameter (Figure 2c). The fiber was heated by a hot-air blower gun (Figure 2b) for 15 s. During the molding procedure, the temperature was maintained below 70  $^{\circ}\text{C}$  so that the fiber melting point would not be reached.

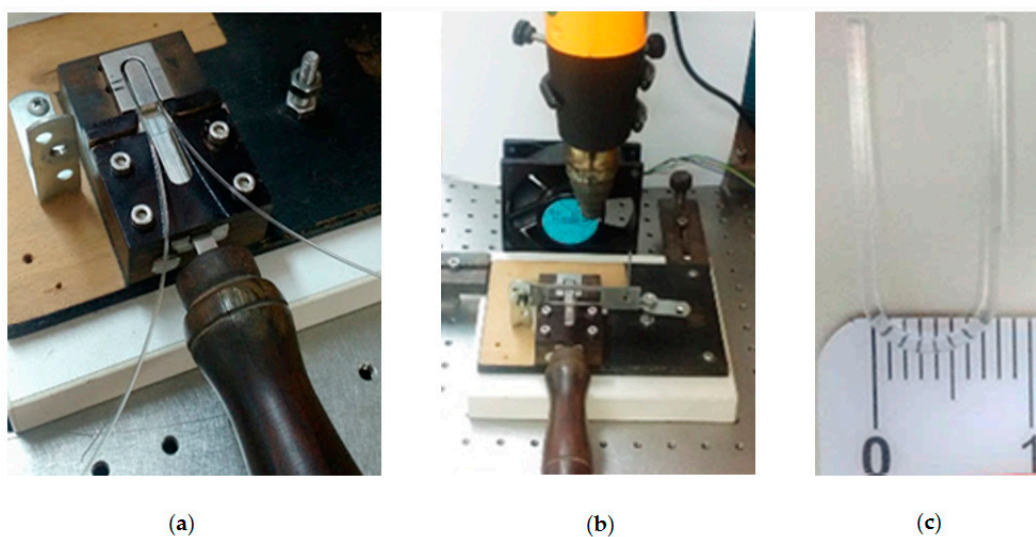


**Figure 2.** (a) Custom-made device used for U-shaped plastic optical fiber (POF) probe molding; (b) Hot-air blower gun used for heating; (c) The finished U-shaped POF fiber with 8 mm in diameter.

A radio-frequency (RF) magnetron sputtering system (Aja International, Scituate, MA, USA) was used for gold thin film deposition on the U-shaped probe surface (Figure 3). A 40 W RF power was applied to ionize the argon gas (plasma) inside the vacuum sputtering chamber. The argon flow rate was maintained at 12 sccm (standard cubic centimeters per minute) at a pressure of  $4 \times 10^{-3}$  mbar. The gold target size was 25.4 mm in diameter and 0.3 mm in thickness.

After molding, the U-shaped probes were cleaned with isopropyl alcohol for two minutes (not exceeding this time in order to avoid fiber cracking), washed in ultrapure water, and dried with ultrapure nitrogen. Then, they were attached to an acrylic support fixed in the substrate holder 10 cm above the gold target and tilted 45 $^{\circ}$  from vertical, as showed in Figure 3a. The substrate holder was rotated at 20 rpm during the deposition process to improve film thickness uniformity. Under these conditions, the gold deposition rate is about 3.5 nm/min and layers of 3.5, 7.0, 10, 18, 30, 50, 70, and 100 nm were deposited in several U-shaped probes (Figure 3b). Notice that due to the fiber cylindrical geometry, the film deposition was not uniform.

After deposition, probes ends were cleaved with the device showed in Figure 3c and polished with a 3- $\mu\text{m}$  polish film as illustrated in Figure 3d.

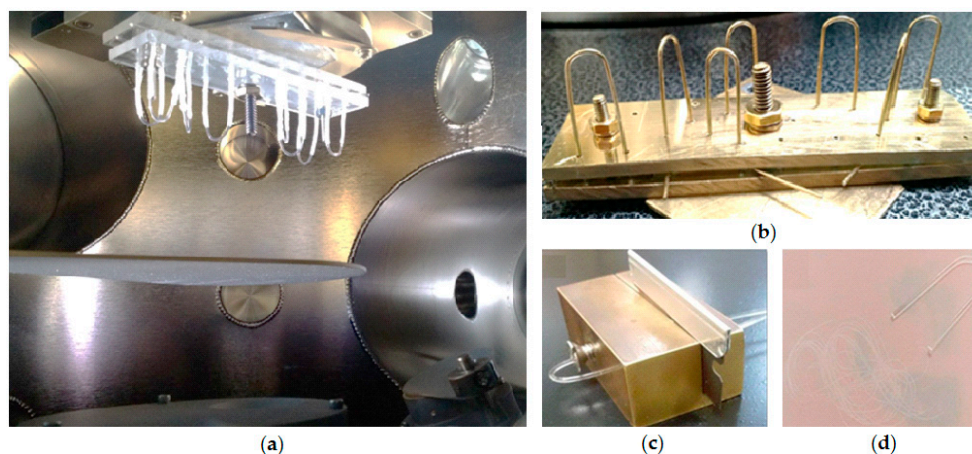


**Figure 3.** (a) Bare U-shaped POF probes installed inside the vacuum sputtering chamber 10 cm above gold target and tilted 45° from vertical; (b) U-shaped POF probes coated with 70 nm gold thin film; (c) Custom-made device used to cleave the probe ends; (d) End faces were polished with a 3  $\mu\text{m}$  polish film in “figure of eight” movements.

### 3.2. Optoelectronic Setups

Two optoelectronic setups were developed. Setup 1 consisted of an 880 nm LED (SFH485P, Siemens) as light source driven by a current source controlled by an Arduino Uno microcontroller. The reason for using an IR light source was to match with the highest sensitivity of the Si photodetector. The light transmitted by the U-shaped POF probe was received by a photodiode, also processed by the microcontroller. Both the LED and the photodiode were encapsulated in an opaque casing to avoid external interference and light leakage of the system.

The Arduino communicates via USB port with a microcomputer, in which there is a digital processing software. The Setup 1 allows simultaneous reading of two sensors in order to allow one of them to be used as a reference sensor without antibody immobilization, and the other one as a bacteria sensor for comparative effect. Setup 1 block diagram and its picture are shown in Figure 4a,b, respectively.

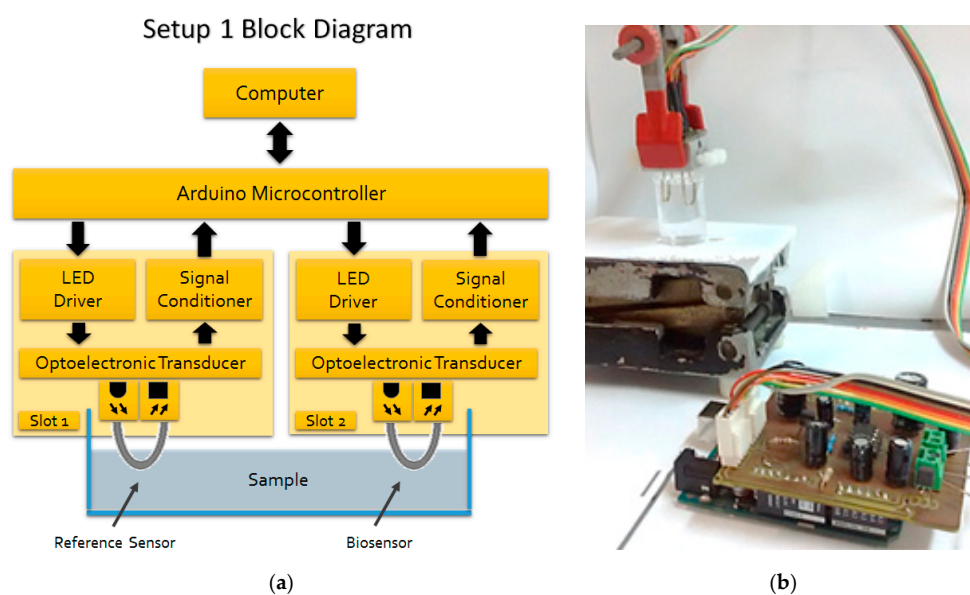


**Figure 4.** (a) Setup 1 block diagram. There are two slots, one for the reference sensor and the other one for the bacteria sensing sensor; (b) Setup 1 picture.

Setup 2 consisted of a 350–845 nm spectrometer and a white light source (HR-4000, HL-2000, Ocean Optics, Winter Park, FL, USA) connected at each end of the U-shaped probe. The reason for adopting Setup 2 (with white light source and a monochromator) was to check for the best wavelength, as Setup 1 used an 880 nm LED.

The Setup 2 block diagram and its picture are shown in Figure 5a,b, respectively.

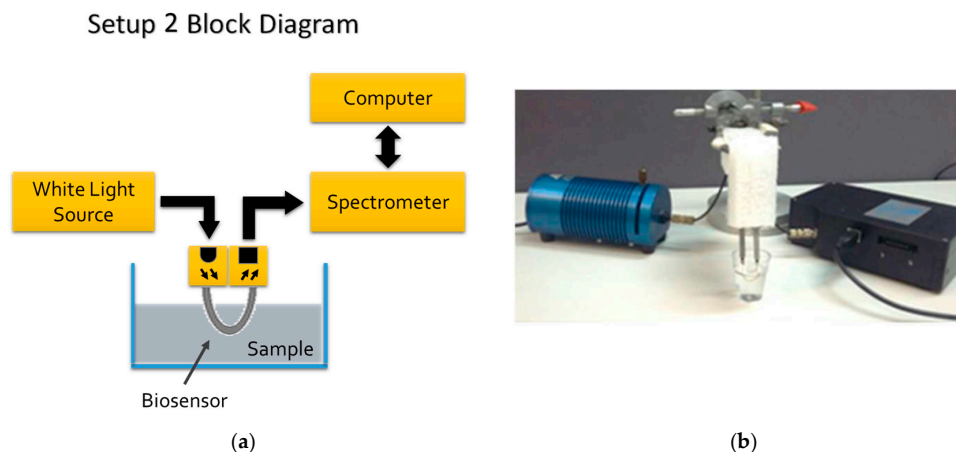


**Figure 5.** (a) Setup 2 block diagram; (b) Setup 2 picture. The white light source is at the left and the spectrometer at the right.

### 3.3. Sucrose Solutions for RI Testing

Aqueous sucrose solutions with RI varying from 1.33–1.39 were prepared in ultrapure water for evaluating sensors sensitivity and repeatability. The solutions refractive index was measured at 589 nm wavelength by an Abbe refractometer (Q767BD, Quimis, Diadema, SP, Brazil) with an uncertainty of 0.0002 refractive index unit (RIU).

The gold-coated U-shaped probes with gold thickness of 18 nm or less were tested with the Setup 1 in eight sucrose solutions with RI varying from 1.33–1.39, randomly. For each concentration, 20 readouts were taken. In turn, the gold-coated U-shaped probes with gold thickness of 30 nm or more were tested in five sucrose solutions, also randomly. Twenty readouts were carried out for each concentration.

With Setup 2, gold-coated U-shaped probes with 10 nm and 70 nm gold thicknesses were tested in six sucrose solutions with RI varying from 1.33–1.39, randomly. For each concentration, 30 readouts were taken.

Straight lines were fitted to experimental data by linear regression for determining a best linear relationship for sensor response versus RI. The expanded uncertainties with 95% confidence level were obtained by the mean standard deviations multiplied by the Student's *t*-distribution *k*-factors, referring to the degrees of freedom used in the tests.

### 3.4. Antibody Immobilization Protocol

The U-shaped POF probes were immobilized with rabbit anti-*Escherichia coli* polyclonal antibody (Bio-Rad, Hercules, CA, USA). The antibody immobilization protocol was adapted from [35], which is briefly described here.

First, the probes were cleaned in isopropyl alcohol P.A. for 2 min and after that in ultrapure water. Then, the bends of the probes were immersed in a 4 mM cysteamine solution for 1.5 h. In this step, thiol (-SH) functional groups of cysteamine molecule bind exchangeable with gold surface through strong ion-exchange interactions. Thereafter, the probes were washed first with absolute ethyl alcohol and then in ultrapure water twice.

The next step was the immobilization of the antibodies by binding the cysteamine amine ( $-\text{NH}_2$ ) functional groups to the carboxylic acid ( $-\text{COOH}$ ) functional groups present in the *E. coli* antibodies. In order to do so, a solution of 100 mM 1-Ethyl-3-(3-dimethylaminopropyl) carbodiimide (EDAC) and 40 mM *N*-Hydroxysuccinimide (NHS) was dissolved in 10 mM phosphate-buffered saline (PBS). Soon after, an antibody concentration of 10  $\mu\text{g}/\text{mL}$  was added in the solution and left to rest during 15 min for activation of the carboxylic acid groups. Thereafter, the probes functionalized with cysteamine were immersed in this solution and left for 1 h for antibody immobilization.

Then, the probes with antibodies were immersed in a 10 mM bovine serum albumin (BSA) solution and left for 30 min in order to block unreacted cysteamine amine functional groups. The removal of unbound reagents is of great importance to avoid non-specific binding thereby reducing the selectivity of the sensor. Lastly, the probes were washed in a 10 mM PBS solution three times to remove unbound antibody molecules. PBS, EDAC and NHS were supplied by Sigma-Aldrich and BSA was supplied by Merck.

### 3.5. Bacterial Suspensions and Testing

Cultures of *E. coli* O55 bacteria (Oswaldo Cruz Foundation, Fiocruz, Rio de Janeiro, RJ, Brazil) were grown in tryptone soya agar (TSA). For selectivity tests, cultures of *Enterobacter cloacae*, *Salmonella typhimurium* bacteria (Laboratory of Food Microbiology, UFRJ, Rio de Janeiro, RJ, Brazil) and *Bacillus subtilis* (Oswaldo Cruz Foundation, Fiocruz, Rio de Janeiro, RJ, Brazil), were grown in soybean triptych broth (TSB) and TSA.

Bacterial suspensions were prepared using ultrapure water and NaCl P.A. (Synth, Brazil). The concentrations were determined using the McFarland 0.5 turbidity standard by visual comparison which correspond to a *E. coli* concentration of  $1.5 \times 10^8$  CFU/mL [36,37] and confirmed by absorbance measurements in the spectrophotometer (UV-1800, Pro-Tools, Porto Alegre, RS, Brazil). The McFarland 0.5 scale has an absorbance value between 0.08 and 0.1 for a wavelength of 625 nm and optical path of 1 cm [36,37]. All bacterial suspensions were prepared using a solution of 0.85% sodium chloride.

Bacteria suspensions with concentrations from  $10^3$ – $10^8$  CFU/mL were prepared for testing the biosensors. In the Setup 1, the gold-coated U-shaped probes with 10 nm and 70 nm thicknesses were immersed into a 5 mL beaker with bacteria suspension. A bare U-shaped probe was immersed together to acts as a reference. Readouts were carried out at intervals of 30 s or 1 min for up to 60 min. In Setup 2, just the gold-coated U-shaped probes with 70 nm thickness were tested. Readouts were carried out at intervals of 5 min for up to 60 min.

After the bacterial suspension testing, the sensors were submitted to safranin solution for 5 s for cell coloring. Then, they were washed with ultrapure water and left to dry at room temperature. After drying, the sensors were taken to an optical microscope with a  $40\times$  magnification. Images were produced with a 13-megapixel camera. The bacterial coverage area was estimated by the ImageJ software.

## 4. Results and Discussion

### 4.1. Gold Thin Film Transmittance

The transmittances of the gold thin films were measured by illuminating gold thin films deposited on glass slides using a white light source (UV to NIR). A pristine glass slide was used as reference. On the other side of the slide a spectrophotometer (Evolution 300, Thermo Scientific, São Paulo, SP, Brazil) analyzed the transmitted light. The light beam was perpendicular to the slide.

The results are showed in the Figure 6. Note that the light transmittance of 880 nm wavelength LED used by Setup 1 is less than 1% for thicknesses exceeding 50 nm and greater than 19% for thickness less than 18 nm. Therefore, the probes coated with gold layer with thickness greater than 50 nm would not lose light on the bend since the film transmittance was negligible such that practically all the light would be reflected and remain inside the fiber.

Also, note that the transmittance was at maximum at wavelengths close to 500–520 nm for all thicknesses, which is inherent to the gold nature. Thus, the LED wavelength should be in this range if the sensor works by the effect of bending loss. However, an 880 nm LED was used because it was part of Setup 1, which was already available for use. These results were in accordance with [38].

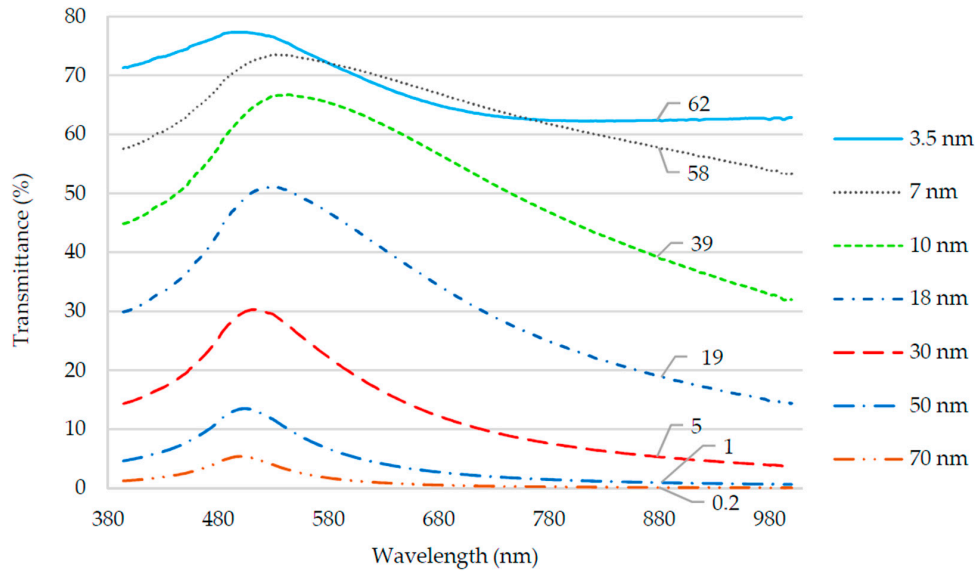


**Figure 6.** Light spectral transmittance of gold thin films. The transmittance values for 880 nm wavelength (light emitting diode (LED) of Setup 1) for each gold film thickness are shown.

#### 4.2. RI Measurements

##### 4.2.1. Sucrose Solutions Testing in Setup 1

Bare and gold-coating U-shaped probes (at least five of each) were tested in sucrose solutions with RI varying from 1.33–1.39 in the Setup 1. The averaged sensor responses are shown in Figure 7. Each dot in the plot is the average of 20 readings. The curve-fitting equations were determined by linear regression.

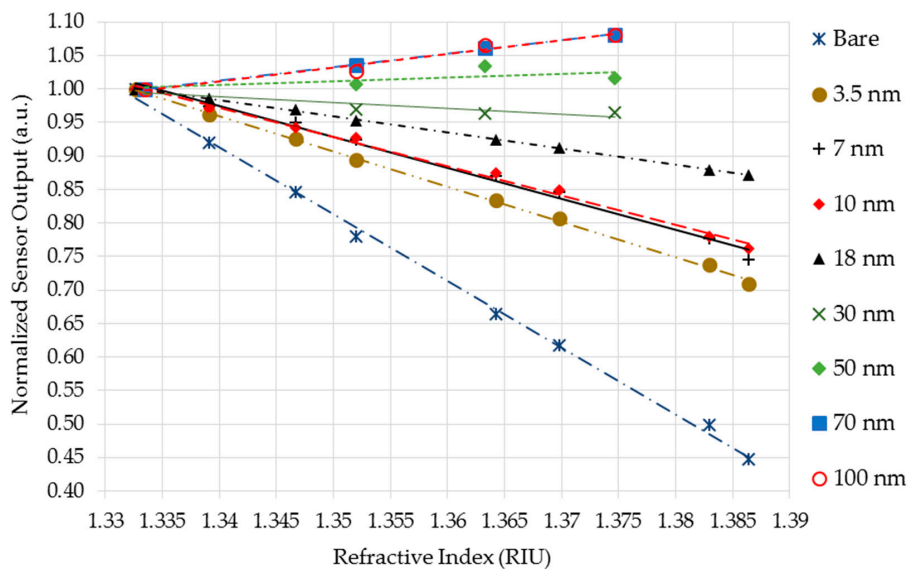


**Figure 7.** Averaged sensor responses for Setup 1 with reflective index (RI) variations for several gold layer thickness.

It can be clearly seen from plots on the Figure 7 that bare U-shaped probes showed a linear relationship between sensor output voltage and sucrose solutions RI for the whole range, indirectly proportional to RI changes, which agreed with the results of [19,23]. The  $R^2$  coefficients were greater than 0.99 for all sensors, which demonstrate a good fit of the linear equations with experimental data. The average sensitivity of the sensors was  $-39.71$  V/RIU with a standard deviation of 2.89 (see Table 1).

**Table 1.** Summary of the biosensors average sensitivities, standard deviations and maximum expanded uncertainties (95% confidence level) in Setup 1.

Old Thickness (nm)	Sensitivity (V/RIU)	Standard Deviation (V/RIU)	Uncertainty (RIU)
0	-39.71	2.89	$3.5 \times 10^{-3}$
3.5	-20.34	2.25	$2.9 \times 10^{-3}$
7	-16.73	2.11	$7.4 \times 10^{-3}$
10	-17.57	2.43	$9.8 \times 10^{-3}$
18	-9.53	1.06	$5.5 \times 10^{-3}$
30	-0.88	-	-
50	0.57	-	-
70	6.01	0.65	$1.9 \times 10^{-2}$
100	8.25	1.05	$7.7 \times 10^{-2}$

It is noticed that the gold-coated U-shaped probes also showed linear relationships of output voltage versus RI for thicknesses up to 18 nm. Notice also that the thicker the layer, the smaller the sensitivity. This is due to the higher reflectivity of thicker layers that decreases the EW interaction with the external medium. Table 1 shows a summary of averaged sensitivity and its standard deviation for each thickness, as well as the maximum expanded uncertainty (95% confidence level) of the inverse regression.

It can be seen that the probes coated with 70 nm and 100 nm presented a linear behavior for the range of 1.33–1.38, but as opposed to the response of sensors with thinner layers, the output rose with the RI. In these sensors, the SPR effect predominated over the bending loss effect in such a way that, as SPR absorption decreased as RI increased, the output light increased more than the losses due to fiber bending. These results were in accordance with [39–41].

Probes with thicknesses between 30 nm and 50 nm were caught in the middle of the two effects, SPR and bending loss. In this region, the two effects competed with each other so that the output light remained constant over the entire RI range.

In summary, for layers up to 30 nm, the dominant effect was the bending loss in which the output light power decreased with an increase of RI, whereas for layers with thickness of 30 nm and above, the dominant effect was the SPR with an increase of output power as RI increased.

#### 4.2.2. Sucrose Solutions Testing in Setup 2

Setup 2, as shown in Figure 8, provided sensor responses for RI variations using Setup 2. Tests with aqueous sucrose solutions were carried out with bare, 10 nm, and 70 nm gold-coated probes. The 10 nm gold-coated probe, in which the effect of bending loss was more pronounced, was chosen because it did not compromise the sensitivity, apart from needing a smaller amount of gold. The 70 nm gold-coated probe, in which the SPR effect was more pronounced, was chosen because it had a reasonable linear response for 1.33–1.38 RI range, and used a smaller amount of gold than the one with 100 nm.

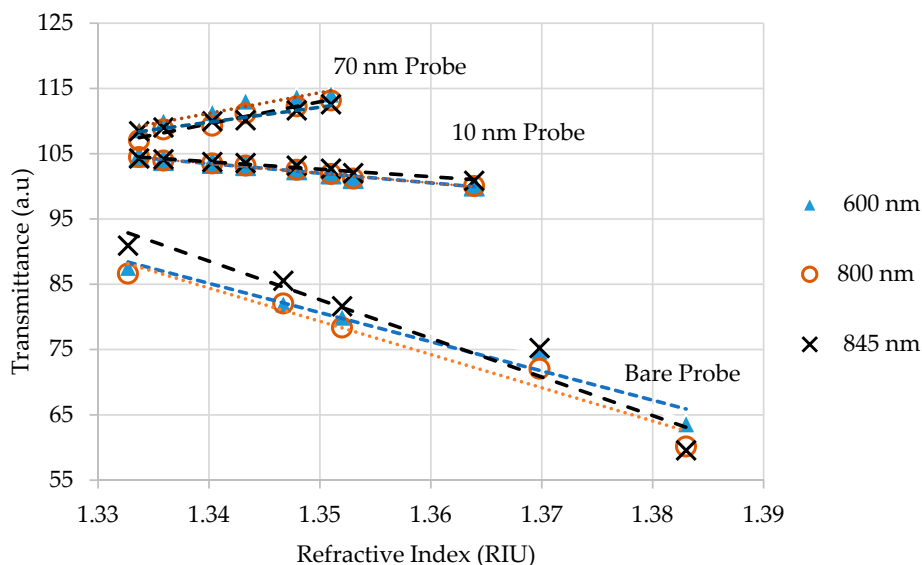


**Figure 8.** Sensor responses for RI variations using Setup 2 for wavelengths 600 nm, 800 nm and 845 nm for bare probe, 10 nm gold-coated probe and 70 nm gold-coated probe.

Figure 8 shows the sensor responses for 600 nm, 800 nm and 845 nm wavelengths. By observing the graph, it can be noticed that the bare probe presented a linear and indirectly proportional relationship between sensor response and RI changes, as expected. The graph shows that the 10 nm gold-coated sensor responses presented the same behavior as the bare probe sensor for a RI range of 1.33–1.38, however, with a lower sensitivity due to the gold layer absorption. Unlike Setup 1, where the sensitivity of 10 nm gold-coated probe dropped by half with the bare probe, in Setup 2, the sensitivity was four times lower.

Figure 8 also shows the 70 nm gold-coated sensors responses that presented the same behavior in Setup 1, linear and directly proportional at RI variations for the range of 1.33–1.352. The sensitivity was better than that of 10 nm gold-coated probe.

Table 2 shows a summary of the sensitivity and maximum expanded uncertainty (95% of confidence level) of the inverse regression for each gold thickness.

**Table 2.** Summary of the biosensors sensitivities and maximum expanded uncertainties (95% confidence level) in the Setup 2.

Gold Thickness (nm)	Sensitivity (1/RIU)	Uncertainty (RIU)
0	−591.78 (845 nm)	$5.8 \times 10^{-4}$
10	−148.66 (600 nm)	$5.1 \times 10^{-4}$
70	338.26 (800 nm)	$5.6 \times 10^{-4}$

#### 4.3. Bacterial Measurements

Probes immobilized with antibodies were tested in different bacterial suspensions in order to evaluate response time and sensitivity for both Setup 1 and Setup 2. For these tests the 10 nm and 70 nm gold-coated U-shaped probes were chosen.

##### 4.3.1. Bacterial Suspensions Testing in Setup 1

Figure 9a,b show respectively, the 10 nm and 70 nm gold-coated sensors responses in Setup 1 for a bacteria concentration of  $1.5 \times 10^8$  CFU/mL. Figure 9c shows the results of 10 nm gold-coated sensor for bacteria concentration of  $1.5 \times 10^6$  CFU/mL. For lower concentrations, either sensors were unable to detect bacteria with the Setup 1.

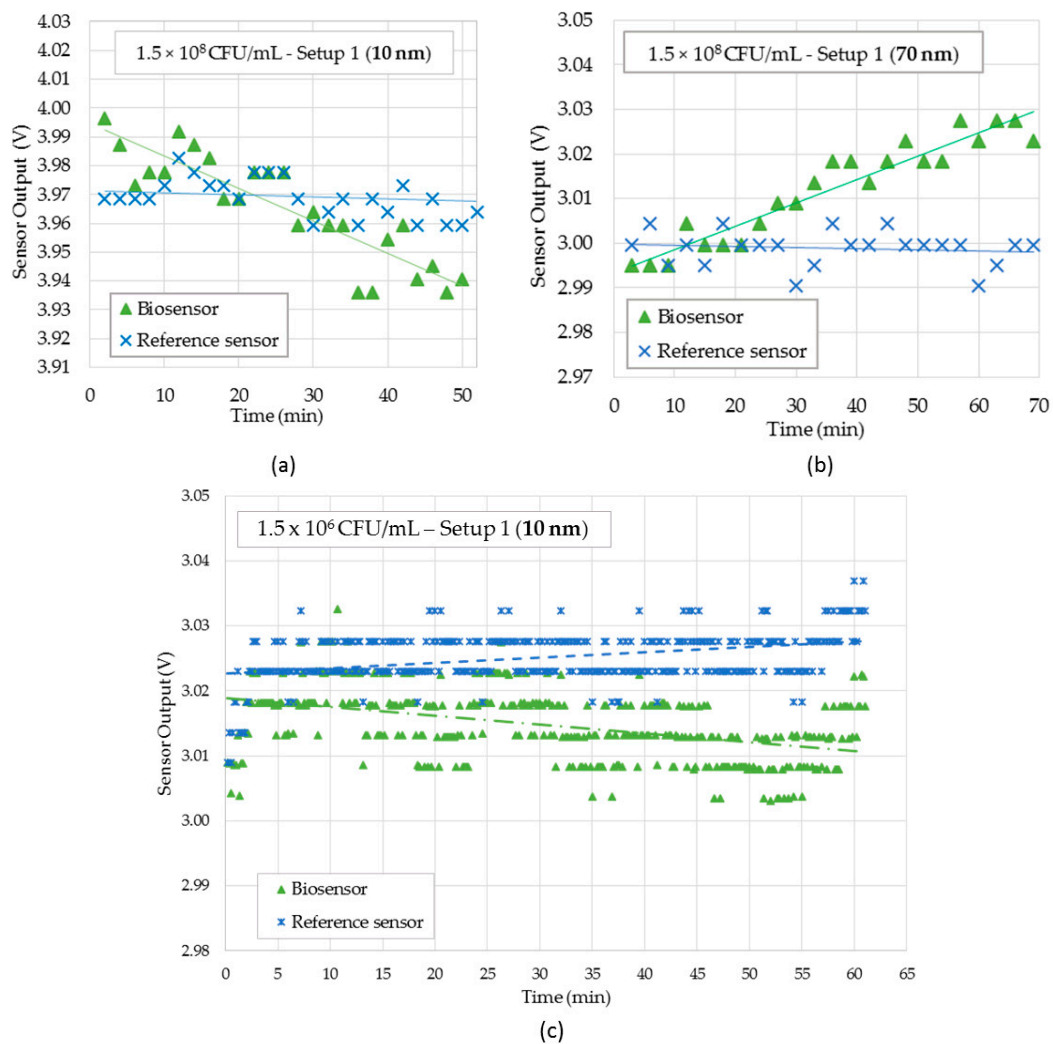


**Figure 9.** Sensor responses for bacterial suspensions using Setup 1. (a) Sensor probe and reference probe for 10 nm gold-coated at  $1.5 \times 10^8$  CFU/mL bacterial suspension; (b) Sensor probe and reference probe for 70 nm gold-coated probes in  $1.5 \times 10^8$  CFU/mL bacterial suspension; (c) Sensor probe and reference for 10 nm gold-coated probes in  $1.5 \times 10^6$  CFU/mL bacterial suspension.

Notice in Figure 9a, that the biosensor output voltage decreased over time due to the increase in the surrounding RI caused by immunocapture effect, as the antibody kept capturing the bacteria present in the water. At the same time, the output voltage of reference sensor remained constant, which confirmed the proper operation of the sensor for bacteria detection. As shown in previous works [19,23], U-shaped probes based on bending loss effect had an indirect relationship between sensor response and RI. Nonetheless, in Figure 9b, the sensor output voltage increased in time as more and more bacteria were bound to sensor surface. This behavior was due to the SPR effect at this specific wavelength, previewed by the experiment shown in Figure 9c. These results are in accordance with [26,27].

Figure 9c shows the sensor output of 10 nm gold-coated U-shaped probe for  $1.5 \times 10^6$  CFU/mL. Notice that the sensor was able to detect this bacterial concentration.

#### 4.3.2. Bacterial Suspensions Testing in Setup 2

For bacterial suspensions testing in Setup 2, 70 nm gold-coated probes were chosen. Figure 10a,b show the sensor responses for bacteria concentration of  $1.5 \times 10^4$  CFU/mL and  $1.5 \times 10^3$  CFU/mL, respectively.

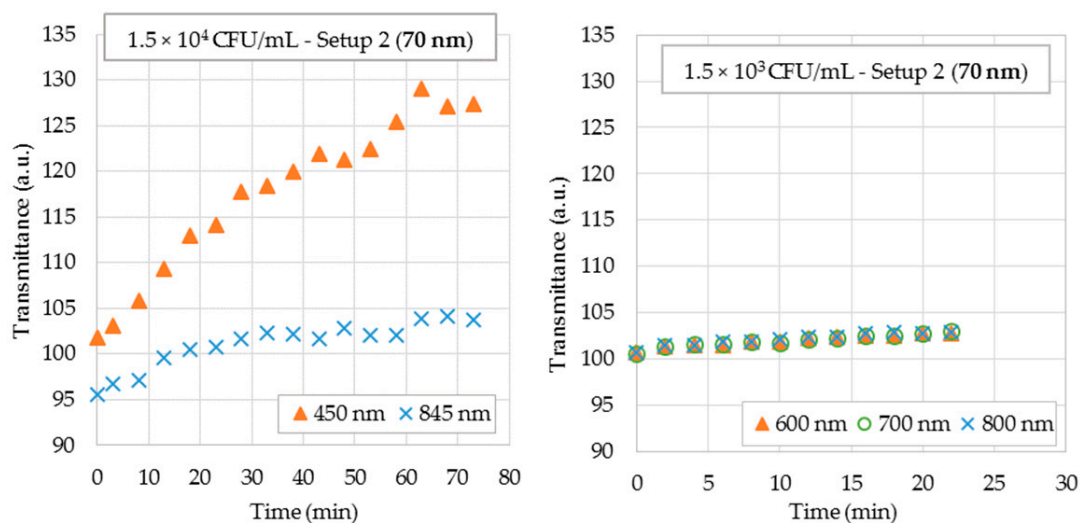


**Figure 10.** Sensor responses for bacterial suspensions using Setup 2. (a) 70 nm gold-coated biosensors in a  $1.5 \times 10^4$  CFU/mL bacterial suspension; (b) 70 nm gold-coated biosensors in a  $1.5 \times 10^3$  CFU/mL bacterial suspension.

Notice in Figure 10 that the sensor was able to detect a concentration of  $1.5 \times 10^3$  CFU/mL. The sensor output voltage increased with time due to the increase in the surrounding RI, as expected. As the response was a transmittance spectrum, it was possible to choose the wavelength in which the sensitivity was higher. Tests with 880 nm were not possible as the wavelength range of the spectrometer is limited to 850 nm. It was shown that the system was capable of providing a positive response to the bacterial concentration in less than 10 min. Notice that the higher the bacteria concentration, the more rapidly the output signal rose.

#### 4.4. Selectivity Testing

In order to verify sensor selectivity, tests were carried out with the bacteria *Enterobacter cloacae*, *Salmonella typhimurium* and *Bacillus subtilis*.

In Figure 11, three 70 nm U-shaped biosensors were tested in the Setup 1 with suspensions of the *Enterobacter cloacae* at high concentration ( $1.5 \times 10^8$  CFU/mL). The graphs show results of each sensor. It is observed that, for a time greater than 40 min, the sensors showed no tendency, meaning that the *E. coli* antibody does not capture this species of bacteria, even in high concentration.

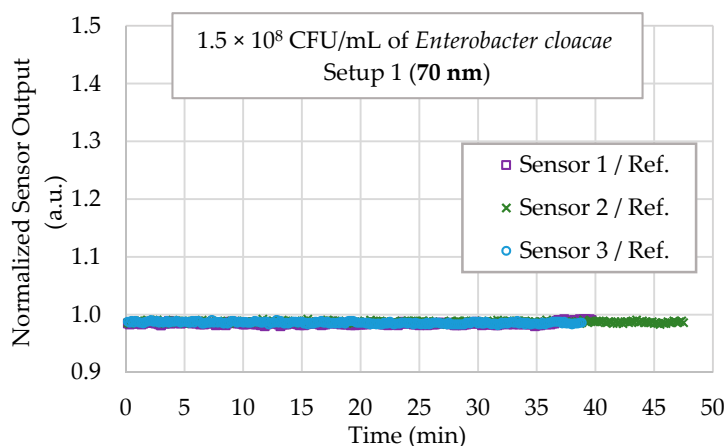


**Figure 11.** Sensor responses for 70 nm gold-coated U-shaped probe for selectivity testing in a  $1.5 \times 10^8$  CFU/mL *Enterobacter cloacae* concentration with Setup 1.

Figure 12a shows the results of the 70 nm probe tested in Setup 2 for *Salmonella typhimurium* suspensions at a concentration of  $1.5 \times 10^8$  CFU/mL. The graphs show the results for 600 nm and 845 nm wavelengths. It is observed that, in this case, the sensor detected the presence of bacteria other than *E. coli*. It is assumed that this occurred due to the antibody being polyclonal rather than monoclonal, which allowed high specificity and lower cross-reactivity.

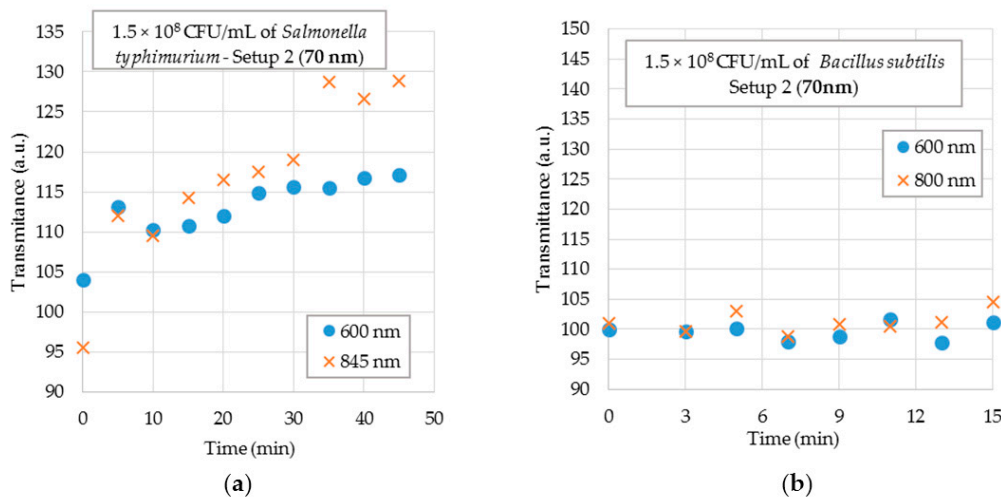


**Figure 12.** Sensor responses for 70 nm gold-coated probe for selectivity testing in a  $1.5 \times 10^8$  CFU/mL bacteria concentration with Setup 2 for 600 nm and 845 nm wavelengths. (a) *Salmonella typhimurium*; (b) *Bacillus subtilis*.

Lastly, Figure 12b shows the results of the 70 nm U-shaped biosensor tested in Setup 2 with *Bacillus subtilis* suspensions at a concentration of  $1.5 \times 10^8$  CFU/mL. The graphs show the results for 600 nm and 845 nm wavelengths. It is observed that there is no tendency, that is, the sensor was not able to capture the bacteria even in high concentration.

#### 4.5. Bacterial Adhesion on Sensor Surface

Figure 13 shows the image obtained by optical microscopy of the bacteria adhesion on the surface of the sensor tested under an *E. coli* concentration of  $1.5 \times 10^8$  CFU/mL. The coverage area estimated by ImageJ software was 16%. This small coverage indicates that immunocapture could be improved to further reduce the detection limit.

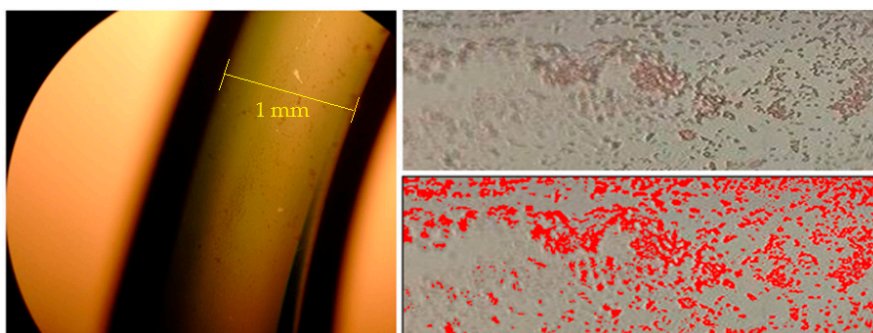


**Figure 13.** Optical microscope image (40 $\times$ ) of *E. coli* coverage over the 70 nm probe after immersion in a bacteria suspension at  $1.5 \times 10^8$  CFU/mL concentration. In left, the probe microscope image. In upper right, a 40 $\times$  magnification image of the bacteria adhered to the fiber surface colored by safranin solution. In bottom right, the coverage area in red estimated by the ImageJ. The coverage area estimated by ImageJ software was 16%.

## 5. Conclusions

A gold-coated U-shaped POF biosensor for *E. coli* detection has been presented. This technique allows using POF as a RI sensor even without removing the cladding.

U-shaped probes coated with gold layers up to 18 nm thick present the same behavior as bare U-shaped probes, in which the bending loss is the sensing predominant effect. Probes coated with 30 nm and 50 nm gold layer are not useful for RI sensing in the range of this application. In 70 nm and 100 nm gold-coated probes, the SPR effect is predominant and the biosensor was capable to detect bacteria concentrations as low as of  $1.5 \times 10^3$  CFU/mL.

In comparing the two employed setups, both detected bacteria. However, Setup 2 was capable to detect up to  $10^3$  CFU/mL, whereas Setup 1 the detection limit was  $10^6$  CFU/mL.

To the best of our knowledge, there are no other works applying POF sensor in bacteria detection. However, in comparing the results obtained in this work with those from our previous publications [15,19], the sensitivity of bare sensor for Setup 1 was slightly better than those from these mentioned works. Additionally, sensors with gold film in Setup 2 also presented a response for lower bacteria concentration ( $10^3$  CFU/mL), whereas in [42] the detection limit was  $10^8$  CFU/mL and in [19] the detection limit was  $10^4$  CFU/mL.

The results demonstrated that the proposed biosensor can be an efficient, low cost, and portable tool for routine analysis of drinkable and bathable water and food quality. This technique can be applied to other types of bacteria by simply immobilizing the antibody of the bacteria to be detected.

In future work, efforts should be devoted to the following aspects: (a) improving the bacteria immobilization and thereby expanding the coverage area on the fiber; (b) a new high-resolution optoelectronic setup operating with an LED with a wavelength that proved to allow greater sensitivity, and (c) selectivity could be improved by using monoclonal instead of polyclonal antibodies.

**Author Contributions:** A.d.S.A. designed and directed the project and performed the experiments; F.d.S.D. helped with the design of experiments (DOE), statistical analysis and writing the chapter about the theory; M.M.W. and R.C.S.B.A. conceived the original idea and were involved in planning and supervising the project. All authors discussed the results and contributed to the final manuscript.

**Conflicts of Interest:** The authors declare no conflicts of interest.

## References

1. Lin, C.-T.J.; Jensen, K.L.; Yen, S. Determinants of Consumer Awareness of Foodborne Pathogens. In *AAEA Annual Meeting*; AAEA: Denver, CO, USA, 2004; pp. 1–4.
2. Lu, L.; Jun, S. Evaluation of a microwire sensor functionalized to detect *Escherichia coli* bacterial cells. *Biosens. Bioelectron.* **2012**, *36*, 257–261. [[CrossRef](#)] [[PubMed](#)]
3. Havelaar, A.H.; Brul, S.; de Jong, A.; de Jonge, R.; Zwietering, M.H.; ter Kuile, B.H. Future challenges to microbial food safety. *Int. J. Food Microbiol.* **2010**, *139*, S79–S94. [[CrossRef](#)] [[PubMed](#)]
4. Júnior, A.I.; Belotto, A.J.; Dhalia, C.B.C. *Manual Integrado de Vigilância, Prevenção e Controle de Doenças Transmitidas por Alimentos*; Ministério da Saúde: Brasília, Brazil, 2010. (In Portuguese)
5. Ana Regina de Freitas, A. *Doenças Alimentares de Origem Bacteriana*; Universidade Fernando Pessoa: Porto, Portugal, 2012. (In Portuguese)
6. General Information | *E. coli* | CDC. Available online: <https://www.cdc.gov/ecoli/general/index.html> (accessed on 15 September 2017).
7. World Health Organization. *Guidelines for Drinking-Water Quality*; World Health Organization: Geneva, Switzerland, 2008; Volume 1.
8. Locking, M.E.; O'Brien, S.J.; Reilly, W.J.; Wright, E.M.; Campbell, D.M.; Coia, J.M.; Browning, L.M.; Ramsay, C.N. Risk Factors for Sporadic Cases of *Escherichia coli* O157 Infection: The Importance of Contact with Animal Excreta. *Epidemiol. Infect.* **2001**, *127*, 215–220. [[CrossRef](#)] [[PubMed](#)]
9. Santos, A.d.; da Silva, J.J.; Bueno, P.R.; Watanabe, A.M. Determinação dos parâmetros cinéticos e termodinâmicos da adsorção de L-cisteína em ouro por meio da técnica de microbalança a cristal de quartzo. *Quím. Nova* **2012**, *35*, 1365–1368. (In Portuguese) [[CrossRef](#)]

10. Lim, J.Y.; Yoon, J.W.; Hovde, C.J. A Brief Overview of Escherichia coli O157:H7 and Its Plasmid O157. *J. Microbiol. Biotechnol.* **2010**, *20*, 5–14. [[PubMed](#)]
11. Tortora, G.J.; Funke, B.R.; Case, C.L. *Microbiologia*, 10th ed.; Grupo A: Artmed, Switzerland, 2000; ISBN 978-85-363-2698-6.
12. Riley, L.W.; Semis, R.S.; Helgerson, S.D.; McGee, H.B. Hemorrhagic Colitis Associated with Rare Escherichia Coli Serotype. *N. Engl. J. Med.* **1983**, *308*, 681–684. [[CrossRef](#)] [[PubMed](#)]
13. Kretzer, J.W.; Biebl, M.; Miller, S. Sample Preparation—An Essential Prerequisite for High-Quality Bacteria Detection. In *Principles of Bacterial Detection: Biosensors, Recognition Receptors and Microsystems*; Springer: New York, NY, USA, 2008; pp. 15–30.
14. Zourob, M.; Elwary, S.; Turner, A. *Principles of Bacterial Detection: Biosensors, Recognition Receptors, and Microsystems*; Springer: New York, NY, USA, 2008; ISBN 978-0-387-75112-2.
15. Beres, C.; Nazaré, F.; Souza, N.; Miguel, M.; Werneck, M. Tapered plastic optical fiber-based biosensor—Tests and application. *Biosens. Bioelectron.* **2011**, *30*, 328–332. [[CrossRef](#)] [[PubMed](#)]
16. Geng, T.; Uknalis, J.; Tu, S.-I.; Bhunia, A.K. Fiber-Optic Biosensor Employing Alexa-Fluor Conjugated Antibody for Detection of Escherichia coli O157H7 from Ground Beef for Four Hours. *Sensors* **2006**, *6*, 796–807. [[CrossRef](#)]
17. Lazcka, O.; Campo, J.; Munoz, F. Pathogen detection a perspective of traditional methods and biosensors. *Biosens. Bioelectron.* **2006**, *22*, 1205–1217. [[CrossRef](#)] [[PubMed](#)]
18. Baccar, H.; Mejri, M.B.; Hafaiedh, I.; Ktari, T.; Aouni, M.; Abdelghani, A. Surface plasmon resonance immunosensor for bacteria detection. *Talanta* **2010**, *82*, 810–814. [[CrossRef](#)] [[PubMed](#)]
19. Wandermur, G.; Rodrigues, D.; Allil, R.; Queiroz, V.; Peixoto, R.; Werneck, M.; Miguel, M. Plastic optical fiber-based biosensor platform for rapid cell detection. *Biosens. Bioelectron.* **2014**, *54*, 661–666. [[CrossRef](#)] [[PubMed](#)]
20. Halkare, P.; Punjabi, N.; Wangchuk, J.; Kondabagil, K.; Mukherji, S. LSPR based fiber optic sensor for detection of E.coli using bacteriophage T4. In Proceedings of the Workshop on Recent Advances in Photonics (WRAP), Bangalore, India, 16–17 December 2015.
21. Balaev, A.E.; Dvoretzki, K.N.; Doubrovski, V.A. Refractive index of Escherichia coli cells. In *Proceedings of SPIE*; SPIE: Bellingham, WA, USA, 2002; Volume 4707.
22. Bryant, F.D.; Seiber, B.A.; Latimer, P. Absolute optical cross sections of cells and chloroplasts. *Arch. Biochem. Biophys.* **1969**, *135*, 97–108. [[CrossRef](#)]
23. Werneck, M.; Lopes, R.; Costa, G.; Rodrigues, D.; Arcas, A.; Dutra, F.; Queiroz, V.; Allil, R. POF Biosensors Based on Refractive Index and Immunocapture Effect. In *Fiber Optic Sensors*; Matias, I.R., Ikezawa, S., Corres, J., Eds.; Springer International Publishing: Cham, Switzerland, 2017; Volume 21, pp. 69–93. ISBN 978-3-319-42624-2.
24. Baccar, H.; Mejri, M.B.; Adams, C.P.; Aouini, M.; Obare, S.O.; Abdelghani, A. Functionalized Gold Nanoparticles for Biosensors Application. *Sens. Lett.* **2011**, *9*, 2336–2338. [[CrossRef](#)]
25. De Carvalho, R.M.; Rath, S.; Kubota, L.T. SPR-Uma nova ferramenta para biossensores. *Quím. Nova* **2003**, *26*, 97–104. [[CrossRef](#)]
26. Navarrete, M.-C.; Díaz-Herrera, N.; González-Cano, A.; Esteban, Ó. A Polarization-Independent SPR Fiber Sensor. *Plasmonics* **2010**, *5*, 7–12. [[CrossRef](#)]
27. Christopher, C.; Subrahmanyam, A.; Sai, V.V.R. Gold Sputtered U-Bent Plastic Optical Fiber Probes as SPR- and LSPR-Based Compact Plasmonic Sensors. *Plasmonics* **2017**. [[CrossRef](#)]
28. Mitsushio, M.; Miyashita, K.; Higo, M. Sensor properties and surface characterization of the metal-deposited SPR optical fiber sensors with Au, Ag, Cu, and Al. *Sens. Actuators Phys.* **2006**, *125*, 296–303. [[CrossRef](#)]
29. Cennamo, N.; Massarotti, D.; Conte, L.; Zeni, L. Low Cost Sensors Based on SPR in a Plastic Optical Fiber for Biosensor Implementation. *Sensors* **2011**, *11*, 11752–11760. [[CrossRef](#)] [[PubMed](#)]
30. Gouveia, C.A.J.; Baptista, J.M.; Jorge, P.A.S. Refractometric Optical Fiber Platforms for Label Free Sensing. In *Current Developments in Optical Fiber Technology*; Harun, S.W., Ed.; InTech: Rijeka, Croatia, 2013; ISBN 978-953-51-1148-1.
31. Chen, C.-H.; Tsao, T.-C.; Tang, J.-L.; Wu, W.-T. A Multi-D-Shaped Optical Fiber for Refractive Index Sensing. *Sensors* **2010**, *10*, 4794–4804. [[CrossRef](#)] [[PubMed](#)]
32. Arrue, J.; Zubia, J. Analysis of the decrease in attenuation achieved by properly bending plastic optical fibres. *IEE Proc. Optoelectron.* **1996**, *143*, 135–138. [[CrossRef](#)]

33. Durana, G.; Zubia, J.; Arrue, J.; Aldabaldetrekue, G.; Mateo, J. Dependence of bending losses on cladding thickness in plastic optical fibers. *Appl. Opt.* **2003**, *42*, 997–1002. [[CrossRef](#)] [[PubMed](#)]
34. Gloge, D. Bending loss in multimode fibers with graded and ungraded core index. *Appl. Opt.* **1972**, *11*, 2506–2513. [[CrossRef](#)] [[PubMed](#)]
35. Celikkol-Aydin, S.; Suo, Z.; Yang, X.; Ince, B.; Avci, R. Sharp Transition in the Immunoimmobilization of *E. coli* O157:H7. *Langmuir* **2014**, *30*, 7755–7761. [[CrossRef](#)] [[PubMed](#)]
36. *BD McFarland Turbidity Standard No 5*; Becton, Dickinson and Company: Sparks, NV, USA, 2010.
37. Zibaii, M.I.; Latifi, H.; Saeedian, Z.; Chenari, Z. Nonadiabatic tapered optical fiber sensor for measurement of antimicrobial activity of silver nanoparticles against *Escherichia coli*. *J. Photochem. Photobiol. B* **2014**, *135*, 55–64. [[CrossRef](#)] [[PubMed](#)]
38. Axelevitch, A.; Apter, B.; Golan, G. Simulation and experimental investigation of optical transparency in gold island films. *Opt. Express* **2013**, *21*, 4126–4138. [[CrossRef](#)] [[PubMed](#)]
39. Ronot-Trioli, C.; Trouillet, A.; Veillas, C.; Gagnaire, H. Monochromatic excitation of surface plasmon resonance in an optical fibre refractive-index sensor. *Sens. Actuators* **1996**, *54*, 589–593. [[CrossRef](#)]
40. Trouillet, A.; Ronot-Trioli, C.; Veillas, C.; Gagnaire, H. Chemical sensing by surface plasmon resonance in a multimode optical fibre. *Pure Appl. Opt. J. Eur. Opt. Soc. Part A* **1996**, *5*, 227. [[CrossRef](#)]
41. Kurihara, K.; Nakamura, K.; Suzuki, K. Asymmetric SPR sensor response curve-fitting equation for the accurate determination of SPR resonance angle. *Sens. Actuators B Chem.* **2002**, *86*, 49–57. [[CrossRef](#)]
42. Rofrigues, D.M.C.; Lopes, R.N.; Franco, M.A.R.; Werneck, M.M.; Allil, R.C.S.B. Sensitivity Analysis of Different Shapes of a Plastic Optical Fiber-Based Immunosensor for *Escherichia coli*: Simulation and Experimental Results. *Sensors* **2017**, *17*, 2944. [[CrossRef](#)] [[PubMed](#)]



© 2018 by the authors. Licensee MDPI, Basel, Switzerland. This article is an open access article distributed under the terms and conditions of the Creative Commons Attribution (CC BY) license (<http://creativecommons.org/licenses/by/4.0/>).